SCIENCE CHINA
Earth Sciences

•RESEARCH PAPER•

October 2021 Vol.64 No.10: 1619–1632
https://doi.org/10.1007/s11430-020-9762-0

Understanding the role of SST anomaly in extreme rainfall of 2020 Meiyu season from an interdecadal perspective

Yuanyuan GUO[1†], Ruijie ZHANG[1†], Zhiping WEN[1,2,3*], Juncong LI[1], Chao Zhang[1] & Zijiang ZHOU[4]

[1] *Department of Atmospheric and Oceanic Sciences & Institute of Atmospheric Sciences, Fudan University, Shanghai 200438, China;*
[2] *Innovation Center of Ocean and Atmosphere System, Zhuhai Fudan Innovation Research Institute, Zhuhai 518057, China;*
[3] *Jiangsu Collaborative Innovation Center for Climate Change, Nanjing 210023, China;*
[4] *National Meteorological Information Center, Beijing 100081, China*

Received November 18, 2020; revised January 12, 2021; accepted March 29, 2021; published online May 25, 2021

Abstract Extreme Meiyu rainfall in 2020, starting from early June to the end of July, has occurred over the Yangtze River valley (YRV), with record-breaking accumulated precipitation amount since 1961. The present study aims to examine the possible effect of sea surface temperature (SST) on the YRV rainfall in Meiyu season from the interdecadal perspective. The results indicate that YRV rainfall in June exhibits more significant variability on interdecadal time scale than that in July. The interdecadal-filtered atmospheric circulation in June, compared with the counterpart in July, shows a more predominant and better-organized Western North Pacific Anticyclone (WNPAC) anomaly, which could transport abundant moisture to the YRV by anomalous southwesterly prevailing in northwestern flank of anomalous WNPAC. Both observation and numerical experiment indicate that the interdecadal change of the SST anomaly in tropical western Indian Ocean (TWI) from preceding May to June can significantly affect the anomalous WNPAC, leading to enhanced YRV rainfall in June. The TWI SST anomaly shifts from a cold phase to a warm phase around the early 2000s, with a magnitude of 0.7°C in 2020, which implies that such interdecadal warming might partly contribute to the heavy rainfall in June 2020 by providing a large-scale favorable background flow.

Keywords Extreme Meiyu rainfall, Western North Pacific anticyclone, SST anomaly

Citation: Guo Y, Zhang R, Wen Z, Li J, Zhang C, Zhou Z. 2021. Understanding the role of SST anomaly in extreme rainfall of 2020 Meiyu season from an interdecadal perspective. Science China Earth Sciences, 64(10): 1619–1632, https://doi.org/10.1007/s11430-020-9762-0

1. Introduction

Researches on the variability in the Meiyu rainfall are of great scientific and socioeconomic importance since anomalous Meiyu rainfall would cause a serious threat to human living, regional agriculture, economy, and society. In the 2020 Meiyu season (June–July), extreme rainfall events mainly occur in the Yangtze River valley (YRV) (Figure 1a and 1b), which caused devastating flood disaster and huge economic losses over China. According to the China Meteorological Administration (CMA), the YRV in 2020 experienced the heaviest Meiyu rainfall since 1961, with a local rainfall accumulation of 759.2 mm, approximately 1.2 times as much as the climatology (http://www.cma.gov.cn/2011wmhd/2011wzbft/2011wftzb/202008/t20200805_560160.html). Hence, much attention was drawn into an unknown issue, that is, what causes extremely abundant Meiyu rainfall in 2020 over the YRV. A better understanding of the unusual Meiyu rainfall in 2020 is very helpful to improving the extreme rainfall prediction, disaster prevention and reduction in China.

In retrospect, substantive studies have noted that the Meiyu rainfall exhibits significant variability on multi-time

† Contributed equally to this work
* Corresponding author (email: zpwen@fudan.edu.cn)

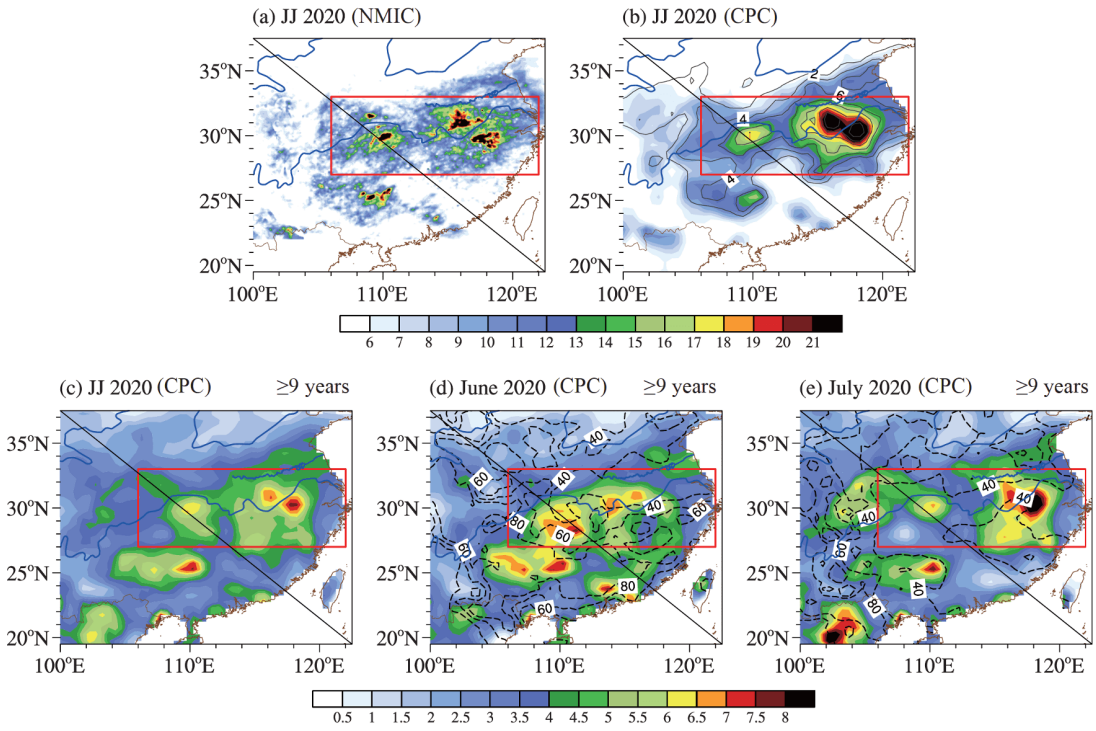

Figure 1 Spatial distribution of June–July-mean precipitation (shaded, unit: mm day^{-1}) in 2020 obtained from (a) the National Meteorological Information Center (NMIC) precipitation dataset merged ground-gauge, satellite and radar, (b) the CPC daily precipitation data. The contour in (b) represents the June–July precipitation anomaly in 2020, starting from 2 mm day^{-1} with an interval of 2 mm day^{-1}. (c)~(e) denote the interdecadal component (shaded, unit: mm day^{-1}) of June–July-mean, June-mean and July-mean precipitation anomaly in 2020. The dash line in (d) and (e), starting from 40% with an interval of 20%, represents the variance contribution (VC) of interdecadal-filtered precipitation anomaly on its totals. The red box denotes the Yangtze River valley (YRV), covering 27°N–33°N, 106°E–122°E.

scale (e.g. Yang and Qian, 2009; Liang and Ding, 2012; Ha et al., 2016; Liang et al., 2018; Ding et al., 2020). In particular, some studies imply that the variation cycles of Meiyu rainfall were concentrated in 10–16 years, 20–30 years and 60–80 years on decadal and interdecadal time scale (Ge et al., 2008; Si et al., 2009; Liang et al., 2018; Sun et al., 2019). For instance, Liang et al. (2018) implies that the interdecadal variation cycles of Meiyu rainfall show a 12–16 years, a quasi 32 years and a quasi 64 years, while Wei and Xie (2005) show that more prevailing cycles of Meiyu rainfall fall in 20 years and 36–38 years. Considering the important contribution of interdecadal component of the Meiyu rainfall on its original variability, how many perturbations of Meiyu rainfall in 2020 can be explained by its interdecadal variation is an interesting issue, however, that remains unknown so far.

Some studies suggest that on the interdecadal time scale, the variations of sea surface temperature (SST) anomaly both on the tropics and mid-high latitudes are tightly connected with the interdecadal perturbations of East Asian summer monsoon (EASM), in particular the Meiyu (Lau et al., 2004; Ding et al., 2010; Liu and Chiang, 2012; Chen et al., 2013; Feng et al., 2014; Zhu et al., 2014; Ha et al., 2016; Si and Ding, 2016). Generally, the Pacific Decadal Oscillation (PDO) (Zhang et al., 1997; Mantua et al., 1997; Mantua and Hare, 2002) shows a positive correlation with the summer rainfall over the YRV since the late 1960s, that is, the warm (cold) phase of PDO is tandem with above (below)-than-normal Meiyu rainfall (Lau et al., 2004; Zhu et al., 2015; Si and Ding, 2016). On the other hand, the basin-scale North Atlantic SST, known as Atlantic Multidecadal Oscillation (AMO) (Schlesinger and Ramankutty, 1994), has a positive correlation with a dipole pattern of summer rainfall in the eastern China. Specifically, the warm (cold) phase of AMO may contribute to the suppressed (enhanced) precipitation over the YRV and enhanced (suppressed) precipitation over Huang-Huai River valley via AMO-North Hemisphere teleconnection (Si and Ding, 2016). In the summer of 2020, the index of PDO is in its cold phase and that of AMO is in its warm phase (figure not shown). According to the studies mentioned above, the 2020 Meiyu rainfall over YRV was supposed to be suppressed by the effect of PDO and AMO on the East Asian summer monsoon. However, the YRV rainfall accumulation in early summer of 2020 broke the historical record since 1961, implying there are some other factors which enhance the Meiyu rainfall over the YRV.

Apart from the effect of PDO and AMO, oceanic forcing in tropical Indian Ocean was also hypothesized to play a role in inducing the interdecadal change of the EASM, especially the summer rainfall (e.g. Ding et al., 2010; Zhang

et al., 2017; Chen et al., 2018; Xie and Wang, 2020). Recently, Xie and Wang (2020) investigated the decadal variation of the Western North Pacific Anticyclone (WNPAC), which plays an important role in connecting the East Asian Meiyu and El Niño-Southern Oscillation (ENSO) (e.g. Fu and Teng, 1988; Zhang et al., 1996; Chang et al., 2000; Wang et al., 2000; Chen et al., 2018). Xie and Wang (2020) claimed that the combined effect of PDO and tropical Indian warming may modulate the decadal variability of WNPAC through changing the Aleutian low and zonal Walker circulation. Hence, on the interdecadal time scale, the SST anomaly in the tropical Indian Ocean has a significant influence on the East Asian Meiyu by modulating the anomalous WNPAC, which provides a possibility that the Indian Ocean SST anomaly may contribute to the record-breaking Meiyu rainfall in the early summer of 2020. Our attention in the present work was devoted into the possible role of SST anomaly both on the tropics and mid-latitudes played to the extremely strong YRV rainfall in 2020 on the interdecadal time scale.

2. Datasets and methodology

2.1 Data

The daily precipitation obtained from Climate Prediction Center (CPC) Global Unified Gauge-Based Analysis from January 1979 to July 2020 at 1.0 degree grid resolution is used in the present study (Xie et al., 2007), which is available at https://psl.noaa.gov/data/gridded/data.cpc.globalprecip.html. The hourly precipitation data merged ground-gauge, satellite and radar with a resolution of 0.05° provided by National Meteorological Information Center (NMIC) from January 2020 to July 2020 (Pan et al., 2015) is only used as a comparison to CPC precipitation data. Monthly mean NOAA Extended Reconstructed Sea Surface Temperature (ERSST) V5 (Huang et al., 2017) was used to proxy the interdecadal change in SST.

Besides, atmospheric circulation was examined using National Centers for Environmental Prediction (NCEP)-U.S. Department of Energy (DOE) reanalysis II (NCEP2) (Kanamitsu et al., 2002) from January 1979 to July 2020 with a horizontal resolution of 2.5° in both zonal and meridional directions, including horizontal wind, air temperature, relatively humidity, geopotential height from 1000 to 300 hPa and vertical velocity at 500 hPa. The specific humidity is calculated by air temperature and relatively humidity at given pressure based on the Clausius-Clapeyron relation, which was performed with NCAR command language (function available at https://www.ncl.ucar.edu/Document/Functions/Built-in/mixhum_ptrh.shtml.). The CPC precipitation, NCEP2 and ERSST datasets are provided by the NOAA/OAR/ESRL PSL, Boulder, Colorado, USA from their website at https://psl.noaa.gov/.

2.2 Methodology

In the present study, the anomalies are obtained by removing the monthly mean climatology for the period of 1979–2020. A harmonic analysis was performed to obtain periods longer than 9 years, in order to focus on the plausible contribution of interdecadal-filtered oceanic forcing on the 2020 extreme rainfall.

The variance contribution (VC), which was used to measure how many variances of total precipitation change can be explained by its interdecadal component, was calculated by the following formula,

$$VC = \frac{\sum_1^N (\widetilde{x_i'})^2}{\sum_1^N (x_i')^2} \times 100\% \quad (i = 1, 2, \ldots N), \tag{1}$$

where x' is the precipitation anomaly from 1979 to 2020 (N =42 years) and the tilde placed over x' represents the interdecadal component of precipitation anomaly after performing the harmonic technique. The VC actually denotes a ratio of the variance of interdecadal-filtered component to the variance of original variable, which is also named as explained variance.

The significance of regression analysis for the interdecadal-filtered anomaly is estimated by the Monte Carlo technique. For example, when the regression method is carried out, one original time series is randomly scrambled. The regression coefficient was calculated between this random time series and other atmospheric field at each grid. We repeated this procedure 1000 times and then sorted these regression coefficients at each grid point in ascending order. If the regression coefficient obtained from the original time series is greater than 97.5% (95%) or smaller than 2.5% (5%) among the quoted regression coefficients at one grid point, then it is significant at 95% (90%) confidence level. Similarly, the correlation coefficient is calculated between the random time series and atmospheric variable, and then its significance is estimated by sorting and comparing these coefficients.

2.3 Model and experiment design

The Community Earth System Model (CESM) is composed of five component models simulating the Earth's atmosphere, ocean, land, land-ice and sea-ice. The Community Atmospheric Model, versions 5.3 (CAM5) is released as part of the atmosphere component of CESM, while CAM5 is also used as a stand-alone model (Neale et al., 2012). In the present work, CAM5 with a horizontal resolution of 0.9° latitude by 1.25° longitude was used to estimate the atmospheric response to the variation of SST in the tropical western Indian Ocean (TWI). Two numerical experiments were conducted for 20 years and the responses of last 15 years were analyzed. In the control run, the climatological

mean annual cycles of global SST and sea ice was imposed on the model. The sensitive run was designed with SST anomalies in the TWI only (TWI_run), in which the inter-decadal-filtered SST warming were imposed in the TWI (15°S–15°N, 45°E–80°E) from April to July, for the purpose of figuring out the atmospheric response to the SST change in the TWI domain on the interdecadal time scale.

3. Extreme rainfall over the YRV in 2020 Meiyu season

3.1 Meiyu rainfall over the YRV in 2020 and its associated atmospheric circulation

Based on the observational precipitation data, abundant rainfall mainly takes place over the middle-lower YRV in June and July of 2020 (Figure 1a and 1b). The high consistence of the precipitation datasets provided by CMA and CPC is suggestive of a good quality of CPC precipitation analysis. Hence, CPC precipitation data was used to be a reliable proxy for measuring the change of Meiyu rainfall hereinafter.

The area-averaged rainfall anomaly over the YRV (27°N–33°N, 106°E–122°E, highlighted in Figure 1) was defined as an YRV rainfall index (YRVRI) in Meiyu season, which is shown in Figure 2a. It is apparent that the normalized June-July-mean YRVRI in 2020 is approximately more than two times that in 1998 and 2016, suggesting an extremely strong Meiyu rainfall in 2020. Historically, devastating flood, such as those in 1998 and 2016, occurred near the YRV (Figure 3). The comparison of these top-3 strongest Meiyu events (that is, 1998, 2016 and 2020) further illustrates the uniqueness of 2020 Meiyu rainfall (Figure 1b and Figure 3), which calls for an urgent need to figure out what causes this extremely rainfall and improve the prediction of extreme rainfall events in China.

Figure 4a shows the daily rainfall accumulation over the YRV from May 1st to July 31th. The above-than-normal Meiyu rainfall events frequently take place after June 2nd and heavy rainfall events persist until the end of July. Obviously, more extreme rainfall events occur in July, instead of June. It is consistent with the observation that the increasing rate of cumulative precipitation amount over the YRV in July 2020 is much larger than that in June 2020 (Figure 4b). Liu et al. (2020) declared that the Meiyu rain-band in June 2020 is induced by a warm front related with a positive phase of North Atlantic Oscillation (NAO), while the rainfall in July is a cold-front-related rainband with a negative NAO. It also suggests that the characteristic and mechanism responsible for the enhanced Meiyu rainfall in June and July of 2020 might be very different.

To illustrate the moisture supply in June and July of 2020, the anomaly of water vapor flux vertically integrated from

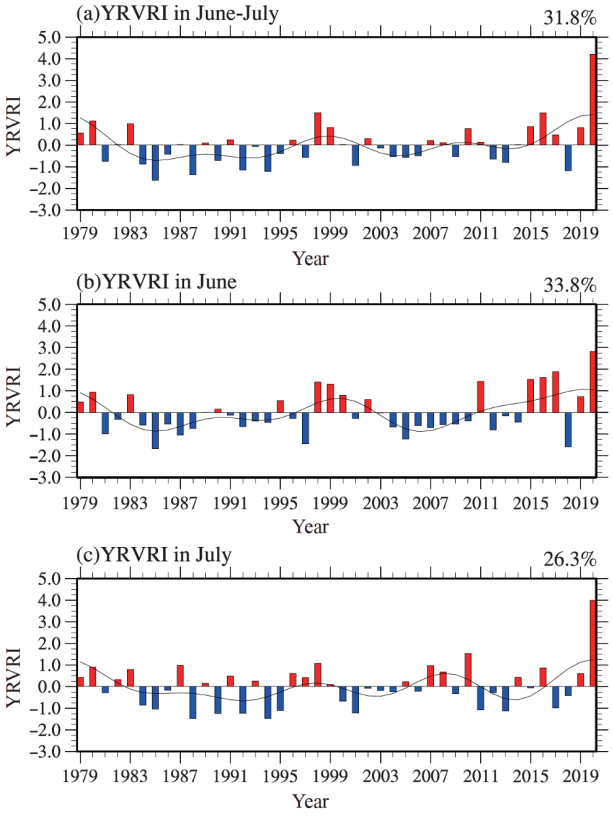

Figure 2 Time series of (a) June-July-mean, (b) June-mean and (c) July-mean normalized YRVRI (bars) and their interdecadal components (black lines) from 1979 to 2020. The variance contribution (VC) of interdecadal components to the total precipitation was given in the top right of each panel.

1000 to 300 hPa and its divergence were shown as Figure 5a and 5b. In June 2020, there are two significant moisture origins. One is the Indochina Peninsula by the anomalous westerly component around 20°N extending from the northwestern continent of Indochina Peninsula (about 90°E) to 110°E, while the other is the northern South China Sea and the southern China south of 25°N (Figure 5a), which is advected by the southwesterly anomaly lying in the northwestern flank of an anomalous WNPAC (Figure 6a). Two water vapor pathways converge to the northeast of Indochina Peninsula and then extend northeast towards the YRV, where remarkable moisture convergence anomaly appears (Figure 5a). Thus, the enhanced water vapor transport directly leads to abundant rainfall over the YRV in June 2020.

In July 2020, a zonal-elongated subtropical high anomaly solidly lies over the South Asia between 10°N–25°N and tilts towards northeast over the western Pacific between 15°N–35°N (Figure 6b). Westerly (southwesterly) anomaly is observed to the north of Bay of Bengal (Indochina Peninsula east of 100°E). Correspondingly, anomalous moisture originating from the South Asian monsoon region near 20°N was transported into the YRV (Figure 5b), which favors the occurrence of heavy rainfall *in situ*. The anomalous subtropical high may hold the key to the moisture supply over

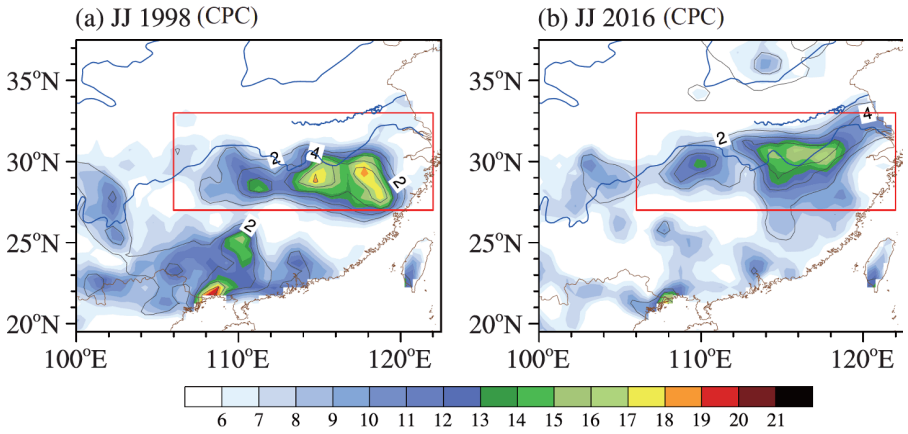

Figure 3 Spatial distribution of June-July-mean precipitation (shaded, unit: mm day^{-1}) and its anomaly (contour, starting from 2mm day^{-1} with an interval of 2mm day^{-1}) in (a) 1998 and (b) 2016 obtained from the CPC daily precipitation data.

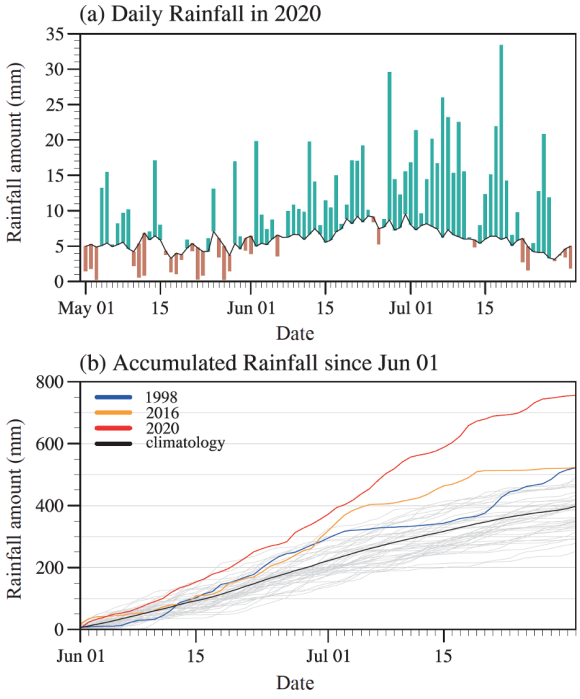

Figure 4 Daily rainfall amount (bars) area-averaged over the YRV from May 1st to July 31th of 2020 (a) and cumulative rainfal area-averaged over the YRV from June 1st to July 31nd from 1979 to 2020 (b). The black curve in (a) denotes the daily climatology of YRV rainfall. The green (brown) bar represents above (below)-than-normal rainfall. The blue, orange, red and gray lines in (b) represent the YRV-averaged cumulative precipitation of 1998, 2016, 2020 and others after 1979. The black line denotes the 42-year averages.

the YRV due to the anomalous southwesterly prevailing to the southwestern flank of anomalous WNPAC, which is closely related to the variation of western Pacific subtropical high. However, differently from the atmospheric circulation in June 2020, there is a noticeable cyclone appearing near the southern Korean Peninsula (Figure 6b), which gives a hint that the mid-latitude circulation may play a more important role in enhancing the Meiyu rainfall in July 2020 than that in June 2020. As Liu et al. (2020) suggests, the Meiyu rainfall starting from June 30th to July 13th of 2020 is associated with the coupling effect of South Asian High and Mongolian Cyclone at the mid-latitude. Nevertheless, our focus is on the effect of anomalous WNPAC, as only the June-mean YRV rainfall shows significant variability on the interdecadal time scale and the mid-latitude cyclone anomaly seemly begins to take effect until July based on our results and Liu et al. (2020).

To clearly reveal the relationship between Meiyu rainfall and the WNPAC, a western North Pacific monsoon index (WNPMI) was used in the present study, which was constructed, following Wang et al. (2001), by the differences of 850hPa zonal wind between 5°N–15°N, 100°E–130°E and 20°N–30°N, 110°E–140°E. A negative (positive) WNPMI represents an anticyclonic (cyclonic) circulation over the western North Pacific, which is related to enhanced (suppressed) rainfall over the YRV in summer (Wang and Lin, 2002). This negative correlation of the WNPAC and summer rainfall over the YRV is also true in the present case, since the correlation between the YRVRI and WNPMI in June (July) is –0.45 (–0.44) (Figure 7a and 7b).

Figure 7c shows the monthly evolution of the anomalous WNPAC in the top-5 heaviest rainfall years (that is, 1980, 1983, 1998, 2016 and 2020, determined by the magnitude of June–July-mean YRVRI, seen in Figure 2a). It turns out that the absolute value of WNPMI in 2020 is largest from May to June among the top-5 heaviest rainfall years, indicating a relatively strongest anticyclonic anomaly over the eastern China in May and June of 2020, which possibly leads to the record-breaking Meiyu rainfall in 2020.

3.2 Interdecadal variability of Meiyu rainfall over the YRV

To address the change of Meiyu rainfall anomaly on the interdecadal time scale, its interdecadal component obtained from a harmonic decomposition removing the periods

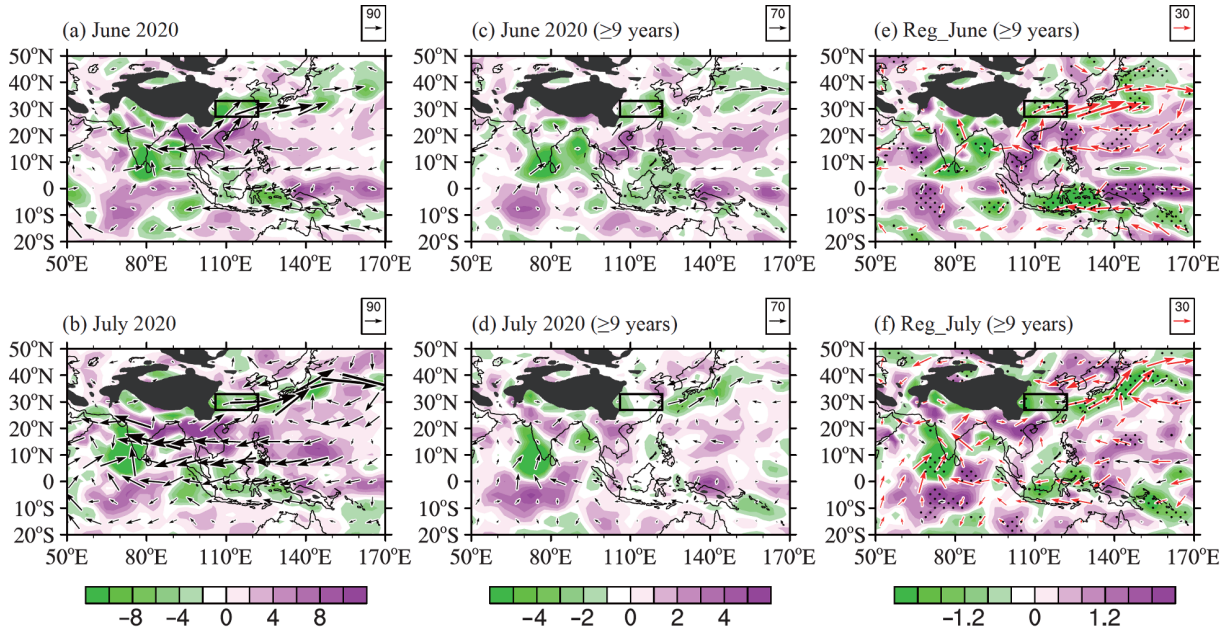

Figure 5 Anomalous vertical integrated water vapor flux (vector, unit: kg m^{-1} s^{-1}) and its convergence (shaded, unit: 10^{-5} kg m^{-2} s^{-1}) (a), (b) and their interdecadal component in (upper) June and (bottom) July of 2020 (c), (d). Regression maps of vertical integrated water vapor flux (vector, unit: kg m^{-1} s^{-1}) and its convergence (shaded, unit: 10^{-5} kg m^{-2} s^{-1}) onto the interdecadal-filtered YRVRI in (upper) June and (bottom) July (e), (f). The red vector (stippling) represents the significance of vertical integrated water vapor flux (its convergence) at the 95% confidence level based on the Monte Carol method. The black boxes denote the target domain of the YRV.

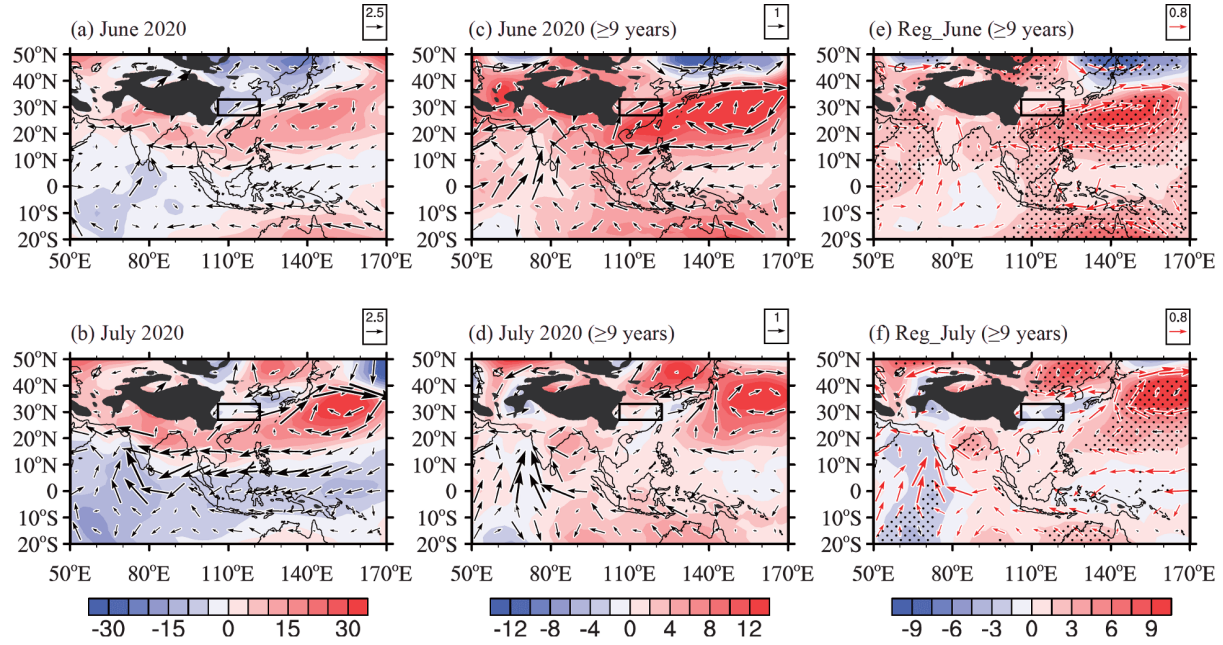

Figure 6 Same as Figure 5, but for anomalous geopotential height (shaded, unit: gpm) and horizontal wind (vector, unit: m s^{-1}) at 850 hPa.

shorter than 9 years was shown as Figure 1c, which is characterized by anomalous heavy rainfall in the eastern China with a maximum near the Anhui Province, resembling the spatial pattern of original rainfall anomaly (contours in Figure 1b). The interdecadal-filtered June–July YRVRI, imposed in Figure 2a, exhibits that its interdecadal component can account for 31.8% of total variance, which is suggestive of a relatively important contribution of its interdecadal component to the total Meiyu rainfall in 2020.

However, the interdecadal component of Meiyu rainfall in June is somehow different from that in July. In June 2020, the maximum anomaly of interdecadal rainfall mainly occurs near the middle-lower YRV and the southern China, while the VC of interdecadal rainfall is almost up to 40% over the

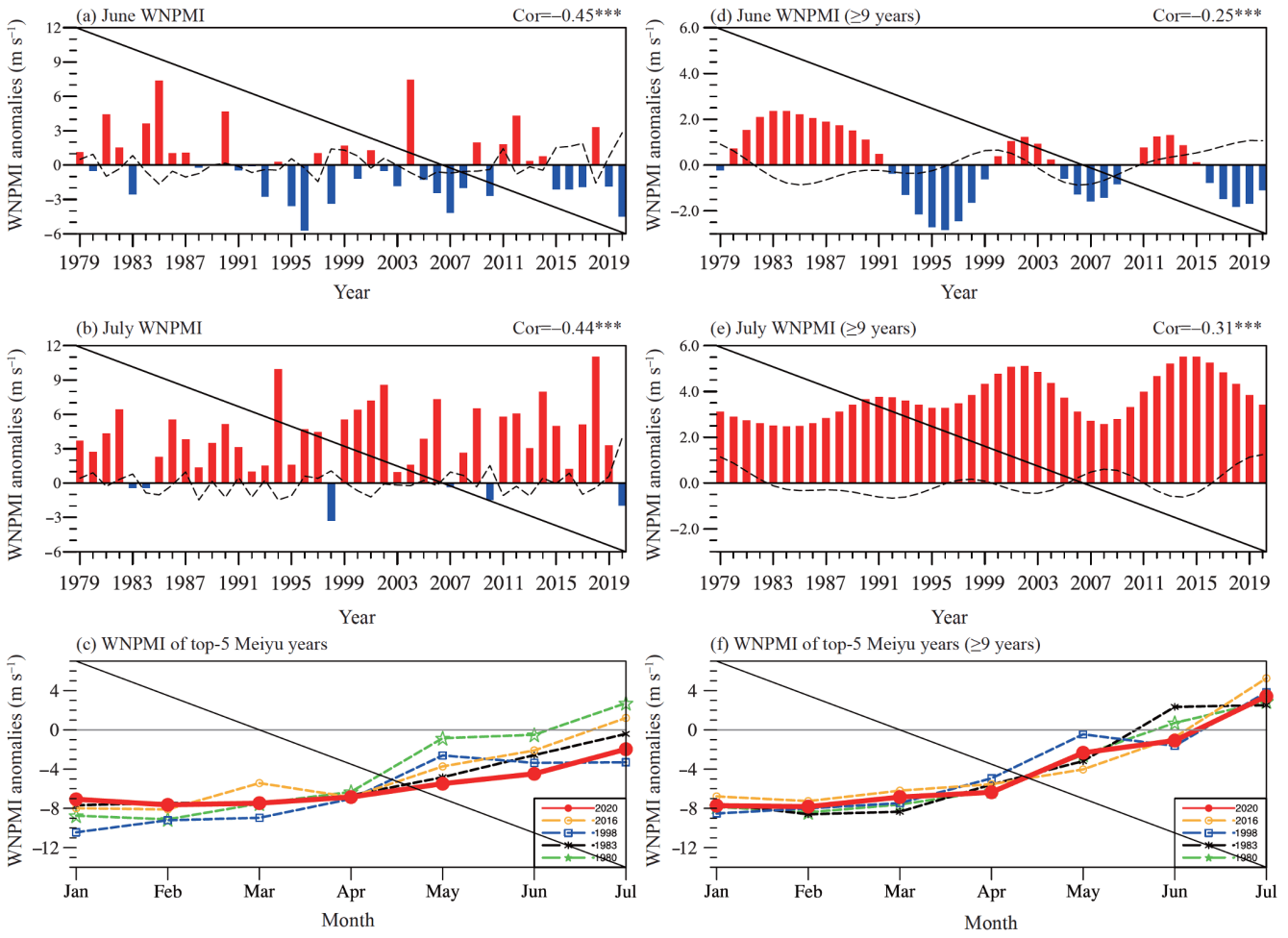

Figure 7 Time series of the WNPMI (bars, unit: m s^{-1}), YRVRI (black dash line) ((a)–(c)) and their interdecadal component in (upper) June and (middle) July ((d)–(f)). The correlation coefficients between the WNPMI and YRV rainfall index are shown in the top right of each panel. The symbols (*, **, ***) in the top right of each panel denote that the value is significant at the 90%, 95% and 99% confidence level estimated by the Monte Carol method. (c), (f) Evolution of the WNPMI and its interdecadal component from January to July for top-5 heaviest rainfall years in the YRV.

YRV (Figure 1d). On the other hand, the interdecadal-filtered rainfall anomaly in July 2020 is basically located near the Hubei, Anhui and Guangxi Province with a maximum center near 30°N and 118°E (Figure 1e). The spatial distribution of VC in July 2020 possesses less than 40% over most area of YRV, which is consistent with the result that the VC (26.3%) of interdecadal-filtered YRVRI in July (Figure 2c) is obviously lower than that in June (33.8%, Figure 2b).

A wavelet analysis was also performed onto the YRVRI in June and July for the period of 1979–2020, respectively (figure not shown) for the purpose of confirming the discrepancies of Meiyu rainfall variation between June and July on the interdecadal time scale. The dominant interdecadal cycle of June-mean YRVRI shows a quasi 18 years, however the July-mean YRVRI cannot exhibit significant period on the interdecadal time scale. This result might suggest that the interdecadal variation of June-mean rainfall over the YRV is more prominent and significant than that of July-mean rainfall.

By looking into the associated interdecadal-filtered atmospheric circulation in June 2020, an apparent anticyclone anomaly solidly lies over the southern China and WNP (Figure 6c), while southwesterly anomaly advects plentiful moisture to the YRV (Figure 5c), which favors the enhanced rainfall in situ on the interdecadal time scale. In July 2020, however, the anomalous anticyclone significantly retreats northeastward and weak northeasterly anomaly is observed over the YRV (Figure 6d), leading to an extremely weak moisture convergence over there (Figure 5d).

To further validate the atmospheric circulation associated with the interdecadal component of Meiyu rainfall over the YRV, the regression analyses upon the interdecadal-filtered YRVRI in June and July were carried out. Associated with interdecadal-enhanced Meiyu rainfall in June, a significant WNPAC anomaly appears over the southern China and WNP (Figure 6e), while the YRV region is covered by significant moisture convergence (Figure 5e), which is similar to the interdecadal component of the atmospheric circulation in June 2020 (Figures 5c and 6c).

Not surprisingly, in terms of the interdecadal-filtered July-mean YRVRI, the regression maps show insignificant easterly anomaly (Figure 6f) and feeble moisture convergence (Figure 5f) near the YRV. By contrast, a predominant cyclonic anomaly appears to the south of Korean Peninsula, accompanied by two significant anticyclonic anomaly centers lying to its northern and eastern flank (Figure 6f), which calls for a need to figure out the plausible effect of the mid-latitude circulation on the Meiyu rainfall in July 2020 in future. However, it is out of our scope.

The interdecadal-filtered WNPMI in June keeps negative after 2015 (Figure 7d), suggesting that the anomalous anticyclonic circulation in the southern China and northern South China Sea becomes stronger since then. On the other hand, the interdecadal-filtered WNPMI in July remains positive during the whole studying period (Figure 7e), which is indicative of an anomalous cyclonic circulation covering the southern China in July on the interdecadal time scale. Assume that the negative correlation between the WNPMI and YRVRI in July is robust and reliable, such cyclonic anomaly over the southern China and northern South China Sea would be suppressed the July-mean YRV rainfall. However, based on the interdecadal-filtered 850hPa atmospheric circulation associated with July-mean YRVRI (Figure 6f), signals are quite weak and insignificant over the southern China. Thus, it is hard to draw a conclusion about the connection between the WNPMI and YRV rainfall in July on the interdecadal time scale, which somewhat gives a hint that the contribution of interdecadal WNPAC variations on the July-mean rainfall over the YRV might be trivial.

To summarize, the results obtained in present suggest that the June-mean YRV rainfall anomaly exhibits a closer and more significant connection with the interdecadal variability of anomalous WNPAC, compared with their connection in July. Hence, more attention would be devoted onto the variation of the June-mean rainfall over the YRV in the following section.

4. Role of SST anomalies on the interdecadal time scale

4.1 Observational results

Since the WNPAC variability is tightly related with the local and remote SST variability (e.g. Wang et al., 2000; Wu et al., 2009, 2010a; Xie et al., 2009), the SST anomaly and 500 hPa vertical velocity anomaly and their interdecadal components were shown as Figure 8. In June 2020, positive SST anomalies are observed in the basin-wide tropical Indian Ocean and western Pacific, accompanied by large-scale ascending anomaly *in situ* (Figure 8a). Meanwhile, a belt-like ascending anomaly appears over the eastern China around 35°N, associated with the strong Meiyu rainband in June 2020. After decomposing the interdecadal components, a similar pattern with warming SST anomalies in the TWI, tropical western Pacific (TWP) and western North Pacific (WNP) is observed in Figure 8b. Note that cooling SST anomalies appear in the southeastern tropical Indian Ocean (Figure 8b), resembling the SST anomaly pattern of Indian Ocean Dipole (IOD) mode (Saji et al., 1999). However, when we performed the regression analysis to the SST anomaly against the interdecadal-filtered YRVRI in June, this IOD-like pattern is not apparent, instead of significant positive SST anomalies centered near 0°, 60°E (Figure 8c).

Moreover, the regressed vertical velocity anomaly at 500 hPa shows relatively weak ascending anomaly in the western and northeastern part of TWI (Figure 8c). In terms of the WNP region, a meridional dipole pattern of vertical velocity anomaly is associated with weak ascending anomaly in the northern WNP and significant descending anomaly in its southern part. There is a tripole pattern of regressed vertical velocity anomaly over the TWP, which is featured by significant descending motion covering the northern and southern TWP domain, together with narrow ascending anomaly along 5°N. It suggests that the warming SST anomalies both in the WNP and TWP may play passive roles that cannot efficiently impact the in-situ atmosphere due to

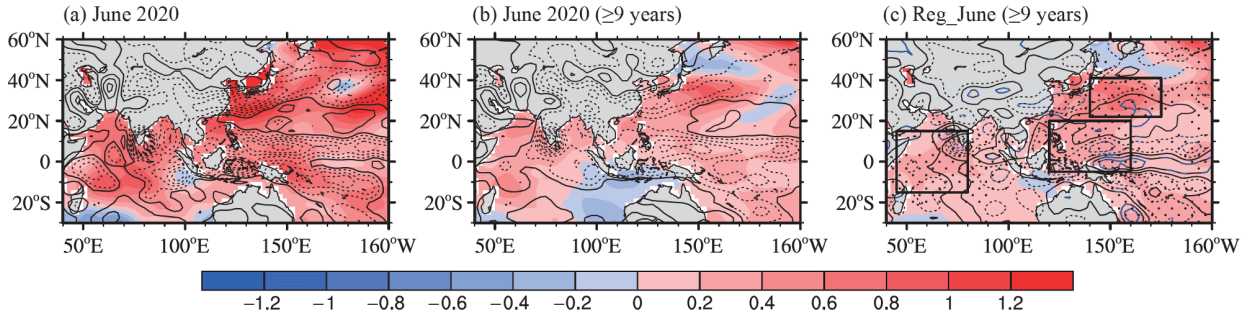

Figure 8 SST anomalies (shaded, unit: °C) and vertical velocity anomalies at 500hPa (contour, unit: Pa s^{-1}) (a) and their interdecadal components in June 2020 (b). Regression map of SST anomalies (shaded, unit: °C) and vertical velocity anomalies at 500 hPa (contour, unit: Pa s^{-1}) onto the interdecadal-filtered YRVRI in June (c). The interval of contour in (a) (b) is 0.03 Pa s^{-1}, staring from 0.01 Pa s^{-1}. The interval of contour in (c) is 0.01 Pa s^{-1}, staring from 0.004 Pa s^{-1}. The stippling (blue contour) represents the significance of SST (vertical velocity) anomalies at the 90% confidence level based on the Monte Carol method. The black boxes in (c) denote the tropical western Indian Ocean (TWI, 15°S–15°N, 45°E–80°E), tropical western Pacific (TWP, 5°S–20°N, 120°E–160°E) and western North Pacific (WNP, 22°N–41°N, 140°E–175°E), respectively.

the local less-significant ascending anomaly.

To further investigate the relationship between the SST anomaly in different key regions and Meiyu rainfall, three SST indices were defined by the area-averaged SST anomalies in the TWI (15°S–15°N, 45°E–80°E), WNP (22°N –41°N, 140°E–175°E) and TWP (5°S–20°N, 120°E–160°E), which were, for the sake of convenience, abbreviated to TWII, WNPI and TWPI hereinafter. A lead-lag correlation analysis was performed between the June-mean YRVRI and three SST indices from preceding January to following July on the interdecadal time scale (Figure 9a).

It was found that the interdecadal-filtered June-mean YRVRI exhibits a highest correlation with the TWII in preceding April with a peak of 0.70 and then its correlation slightly decreases to 0.55 in June, but still significant at 95% confidence level. Although some studies suggest that the Indian Ocean SST forcing in El Niño peak winter and decaying spring can influence the WNP circulation by model simulations (e.g. Watanabe and Jin, 2002), some recent researches argued that the SST anomaly in the Indian Ocean from peak winter to decaying spring might play a passive role which is influenced by the atmospheric circulation, and the SST warming in Indian Ocean helps to maintain the anomalous WNPAC only in El Niño decaying summer (e.g. Wu et al., 2009, 2010a; Li et al., 2017). Sequentially, it is necessary to examine the role played by the TWI SST anomaly from the preceding April to June in the present case.

Figure 10 shows the regressed SST anomaly and vertical velocity anomaly at 500 hPa from April to May onto the interdecadal-filtered YRVRI in June. It was noted a basin-wide warming of Indian Ocean in April, which is accompanied by a northeast-southwest-oriented triple pattern of vertical velocity anomaly with wide descending anomaly in the tropical Indian Ocean between 60°E–85°E, as well as ascending anomaly between 40°E–60°E and east of 90°E (Figure 10a). Hence, the warming SST anomaly in the eastern part of TWI domain (near 70°E) in April might be a result of the atmospheric forcing and the counterpart in the western TWI (near 50°E) may play a relatively active role which influences the atmosphere.

Differently, the SST anomaly in May significantly increases in the TWI with a maximum of 0.3°C locating near 0°, 55°E and the associated vertical velocity anomaly shows a relatively wide ascending motion in the TWI (Figure 10b), which provides a possibility of the active forcing by the TWI SST warming on the atmospheric circulation since May. In simultaneous June, a relatively weak ascending anomaly can be still observed in the most area of TWI (Figure 8c), which indicates that the TWI SST warming from May to June may continuously play an active role on modulating the anomalous descending motion east and northeast to TWI region, which could affect the WNPAC anomaly via changing the vertical circulation. Based on Figure 9b, the TWII in May shifts from a cold phase to a warm phase around the early 2000s, suggesting an interdecadal warming of the TWI SST since then, which may provide a large-scale background flow favoring the frequent occurrence of rainfall over the YRV.

It is worthwhile to mention that the SST warming could be

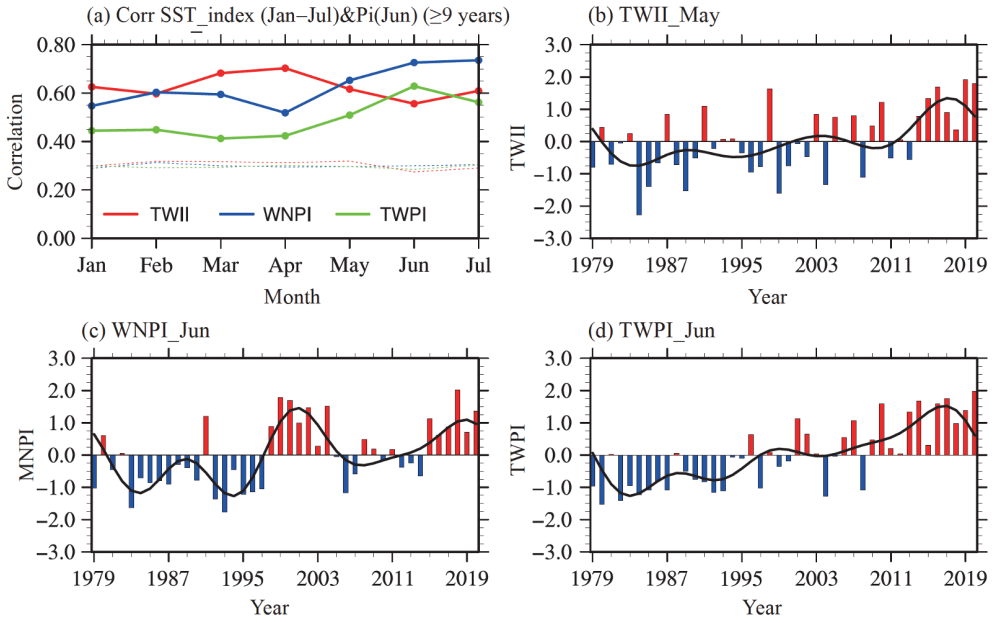

Figure 9 (a) Lead-lag correlation of the YRVRI in June and the SST anomaly indices from the preceding January to following July. (b)–(d) Time series of the normalized TWII in May, WNPI in June and TWPI in June (bars) from 1979 to 2020. The red, blue and green solid lines in (a) represent the area-averaged SST anomaly in the TWI, WNP and TWP, respectively. The dashed lines represent the correlation coefficients that are significant at the 95% confidence level estimated by the Monte Carlo method. The black curves in (b)–(d) denote the interdecadal-filtered SST indices obtained by a harmonic analysis.

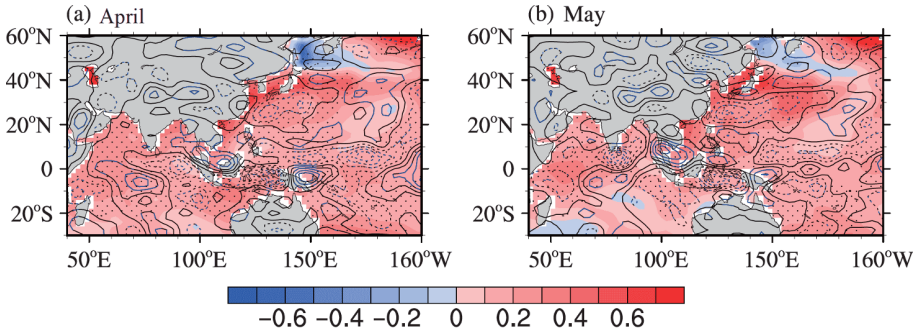

Figure 10 Regression map of SST anomalies (shaded, unit: °C) and 500 hPa vertical velocity anomalies (contour, unit: Pa s^{-1}) in (a) April and (b) May onto the interdecadal-filtered YRVRI in June. The interval of contour is 0.08 Pa s^{-1}. The stippling (blue contour) represents the significance of SST (vertical velocity) anomalies at the 90% confidence level based on the Monte Carol method.

still observed in the TWI in July 2020. However, there is a quite weak WNPAC anomaly appearing east of 120°E, accompanied by a relatively weak cyclone anomaly near Okhotsk Sea in July 2020 (Figure 6d). As Liu et al. (2020) demonstrated, the Meiyu rainfall in July 2020 might be induced by the coupling between the South Asian High and mid-latitude Mongolian Cyclone with a phase shift of NAO around the late June, which suggests a more important contribution of mid-latitude atmospheric circulation on the July-mean Meiyu rainfall than that on the June-mean Meiyu rainfall. Thus, the contribution of TWI SST warming in July might be largely limited.

Apart from the TWII, Figure 9a also shows a tight simultaneous relationship between the June-mean YRVRI and WNPI (TWPI) with a correlation of 0.73 (0.63). The June-mean WNPI and TWPI experienced a relatively warming period since the mid-1990s, however, both of them have rather limited influence on the surrounding atmospheric circulation based on the investigation hereinbefore.

The vertical integrated moisture supply and the lower-tropospheric atmospheric circulation in June associated with the interdecadal-filtered TWII in preceding May, WNPI and TWPI in simultaneous June were examined (Figure 11). Corresponding to a warmer SST anomaly in the TWI region in May, there is a similar SST anomaly pattern in June, indicating a persistent warming in the TWI (figure not shown). Meanwhile, in June there is an anomalous high pressure belt extending from the India to WNP, accompanied by anomalous WNPAC covering the South China Sea and WNP (Figure 11d). To its northwestern edge, southwesterly anomaly dominates in the southern China, which will bring plentiful water vapor to the YRV (Figure 11a) and then lead to above-than-normal rainfall over there. Similarly, associated with a simultaneous warmer WNP (TWP), anomalous subtropical anticyclonic circulation is observed over the western Pacific between 15°N–35°N (5°N–30°N), seen in Figure 11e (Figure 11f). The results show that an anticyclonic anomaly appears underneath the warm SST anomalies, implying that the warming of SST in the WNP and TWP is induced by the local anticyclonic circulation, rather than forcing the atmospheric circulation.

Note that the high similarities among the atmospheric circulations related to a positive TWII, WNPI and TWPI may ascribe to the close correlation among three SST indices, since the correlation coefficients between TWII-WNPI, TWII-TWPI and WNPI-TWPI are 0.48, 0.84 and 0.66, respectively. To isolate the linkage between the SST anomalies in each key region and the anomalous atmospheric circulation, a partial regression analysis was performed (figure not shown). After removing the variation of WNPI and TWPI, the anomalous atmospheric circulation at 850 hPa and vertical integrated moisture supply associated with positive TWII is similar to that in Figure 11a and 11d, suggesting the SST anomaly in the TWI may be independently connected with the anomalous WNPAC and YRV rainfall in June. On the other hand, apart from a significant anomalous anticyclonic circulation covering over the WNP (TWP), the anomalous moisture supply over the YRV are quite weak when we attempt to distinguish the atmospheric circulation associated with WNP (TWP) by partial regression. These results indicate that compared with the WNP and TWP SST anomaly, the TWI SST anomaly may play the most important role in inducing above-than-normal YRV rainfall on the interdecadal time scale.

It should be noted that all three SST indices exhibit a significant warming-trend from 1979 to 2020. The 42-years studying period limits us to clearly determine whether this warming-trend is related with the global warming or it only represents a half-cycle of interdecadal oscillation. To briefly discuss this question, the lead-lag correlation analysis was repeated after removing the long-term trend of each SST index. The correlation between the detrended interdecadal-filtered TWII in May and YRVRI in June is 0.43, significant at 95% confidence level estimated by Monte Coral method. This suggests that the relationship of the YRV rainfall in June and the TWI SST anomaly is still robust after removing the warming trend of SST anomaly.

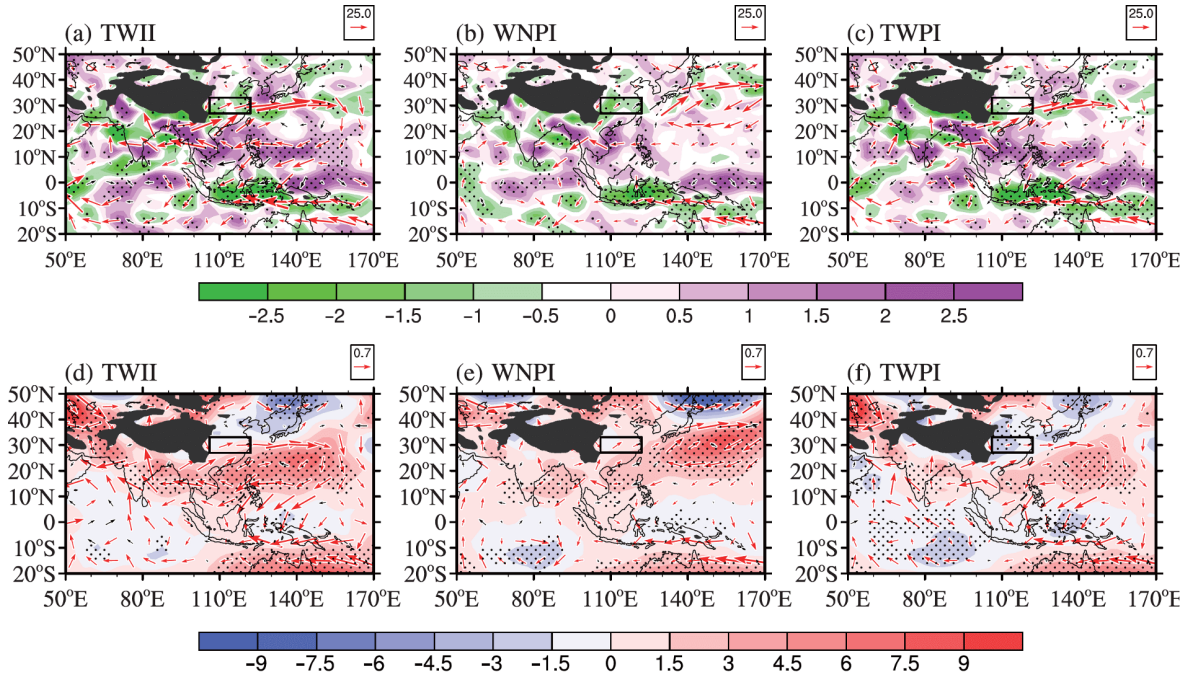

Figure 11 ((a)–(c)) Regression maps of the vertical integrated water vapor flux anomaly (vector, unit: kg m^{-1} s^{-1}) and its convergence (shaded, unit: 10^{-5} kg m^{-2} s^{-1}), ((b)–(d)) 850 hPa geopotential height anomaly (shaded, unit: gpm) and 850 hPa horizontal wind anomaly (vector, unit: m s^{-1}) onto the interdecadal-filtered. (a) (d) TWII in May, (b) (e) WNPI in June and (c) (f) TWPI in June. The stippling and red vectors indicate significance at the 90% confidence level based on the Monte Carol method. The black box represents the YRV region examined in the present study.

4.2 CAM5 experiments

In order to address the impact of the SST anomaly in the TWI on the Meiyu rainfall over the YRV, a sensitive experiment was carried out and related experiment design was introduced in Section 2c. Figure 12 shows the differences of the moisture supply and lower-tropospheric atmospheric circulation between the sensitive and control runs.

In the TWI_run, a belt-like distribution of geopotential height anomaly is observed over the South Asia and western Pacific around 15°N–25°N, with maximum centers lying over the northern Arabian Sea, Bay of Bengal and the east of Taiwan (Figure 12b). Meanwhile, the southwesterly anomaly prevails in the southern mainland of China, bringing abundant water vapor from the South China Sea and the TWP towards YRV (Figure 12a). Overall, the responses of TWI_run are consistent with the observation, confirming the significant effect of TWI SST warming on the YRV rainfall in June. Considering the strong warming of TWI in May 2020 (Figure 9b), it partly contributes to the extreme rainfall over the YRV by providing a favorable background flow from the interdecadal perspective.

Nevertheless, the related moisture convergence anomaly in the TWI_run is centered near 32°N, a little northward than that in the observational result (Figure 11a), which may be partly result from the model basis. For instance, Xie et al. (2016) intend to examine the effect of aerosols on the East Asian summer monsoon and they found that CAM5 would reproduce a stronger and more northward-shifted western Pacific subtropical high in comparison with reanalysis.

5. Summary and discussion

Extreme rainfall events occur over the YRV in June and July of 2020, breaking the historical record provided by the China Meteorological Administration (CMA) since 1961, which causes widespread and devastating floods over the YRV in early summer of 2020. In the present work, we intend to understand the extreme rainfall in 2020 Meiyu season from an interdecadal perspective.

It is found that the YRV rainfall in June shows a more remarkable interdecadal variation compared with that in July. Furthermore, the YRV rainfall in June shows significant positive correlation with the SST variation in the TWI, WNP and TWP on the interdecadal time scale. In particular, the results attest that the TWI SST anomaly in proceeding April has the highest positive correlation with the YRV rainfall in June, but begins to efficiently take effect since May. Specifically, a persistent warming of SST anomaly in the TWI from previous May to simultaneous June would force an anomalous anticyclonic circulation extending from South Asia to the TWP through modulating the vertical meridional circulation over the Monsoon region in June, and eventually enhance the YRV rainfall via transporting plentiful water

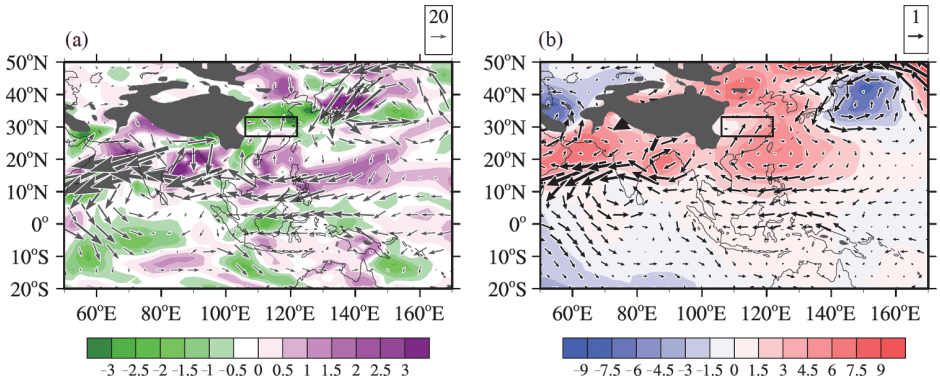

Figure 12 Differences of the (a) vertical integrated water vapor flux anomaly (vector, unit: kg m^{-1} s^{-1}) and its convergence (shaded, unit: 10^{-5}kg m^{-2} s^{-1}), (b) 850 hPa geopotential height anomaly (shaded, unit: gpm) and 850 hPa horizontal wind anomaly (vector, unit: m s^{-1}) between the TWI_run and CAM5 control run.

vapor to the YRV by anomalous southwesterly. The CAM5 experiment with described SST warming in the TWI has confirmed this physical process mentioned hereinbefore. Thus, our present results suggest that the SST variation in the TWI has significant influence on the YRV rainfall in June, in which the anomalous WNPAC acts as a bridge linking the oceanic forcing with Meiyu on the interdecadal time scale.

We also note that the SST anomaly in the TWI shifts from a cold phase to a relatively warm phase after the early 2000s. The SST anomaly averaged in the TWI region in May 2020 exceeds 0.7°C (about 1.8 standard deviation), which might partly enhance the Meiyu rainfall in the early summer of 2020 via affecting the anomalous WNPAC. The present work devotes more attention into the interdecadal variation of June-mean YRV rainfall, however, more extremely strong rainfall events take place in July 2020 (Figure 4a). Hence, we have to recognize that the interdecadal contribution of other factors on the July-mean Meiyu rainfall needs further examination in future.

The interdecadal variability of atmospheric circulation at mid-high latitudes has pronounced influence on the East Asian climate, such as the Silk Road pattern, Pacific-Japan pattern and so on (e.g. Chowdary et al., 2019; Li et al., 2019; Xu et al., 2019). Whether those factors contribute to extreme Meiyu rainfall on the interdecadal time scale still remains unclear. Hence, it is necessary to fully understand this record-breaking rainfall event via estimating the contribution of mid-high-latitudinal systems, in particular for the extreme rainfall events occurring in July 2020.

Additionally, there is a limitation of the used harmonic technique to isolate the interdecadal component of Meiyu rainfall and atmospheric circulation anomalies in the ending point, since 2020 is the end-year of studying period. To discuss the sensitiveness of our results to the filtering technique and the edge limitation, some efforts have been taken in the present study. First of all, a harmonic analysis was repeated onto the June-mean rainfall anomalies with sliding the ending point from 2015 to 2020 (Figure 13a). The differences of values with different ending points mainly exist in their magnitude, however, an interdecadal-wetting of YRV rainfall could be clearly observed using harmonic technique with different ending points.

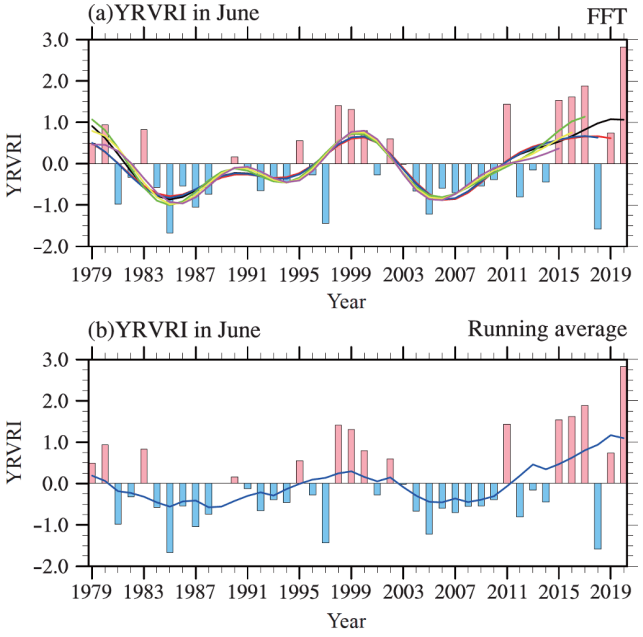

Figure 13 Time series of normalized June-mean YRVRI (bars) and its interdecadal components (lines) filtered by the harmonic analysis (a) and 9-year running mean from 1979 to 2020 (b). The colorful lines in (a) represent the interdecadal-filtered values by sliding the end-point from 2015 to 2019. The blue line in (b) represents the 9-year running average, in which the end-point is calculated by the method introduced in section 5.

On the other hand, a 9-year running mean was performed onto the June-mean rainfall anomalies to estimate the interdecadal components in the present case. For the end points, a method was developed. For instance, the regular points for 1983–2016 were smoothed by the 9-year running window. The value in 2017 was generated by taking the average with an 8-year window, that is from 2013 to 2020. Sequentially, the interdecadal component in 2020 was estimated by the average from 2016 to 2020. By comparison, the value of

normalized June-mean YRVRI in 2020 obtained from the harmonic analysis is approximately 1.06 standard deviation (Figure 13a), while that obtained from the 9-year running mean is 1.10 standard deviation (Figure 13b). The results, to some extent, are not sensitive to the filtering technique. However, the filtering method could be improved in the future studies.

Acknowledgements *The authors thank the constructive suggestions from two anonymous reviewers, which help greatly to improve the manuscript. This research was supported by the National Key R&D Program of China (Grant No. 2016YFA0600601) and the National Natural Science Foundation of China (Grant Nos. 41905072, 41530530 & 41875087).*

References

Chang C P, Zhang Y, Li T. 2000. Interannual and interdecadal variations of the East Asian summer monsoon and tropical Pacific SSTs. Part I: Roles of the subtropical ridge. J Clim, 13: 4310–4325

Chen J, Wang X, Zhou W, Wang C, Xie Q, Li G, Chen S. 2018. Unusual rainfall in Southern China in decaying august during extreme El Niño 2015/16: Role of the Western Indian Ocean and north tropical Atlantic SST. J Clim, 31: 7019–7034

Chen W, Feng J, Wu R. 2013. Roles of ENSO and PDO in the link of the East Asian winter monsoon to the following summer monsoon. J Clim, 26: 622–635

Chen W, Wang L, Feng J, Wen Z, Ma T, Yang X, Wang C. 2019. Recent progress in studies of the variabilities and mechanisms of the East Asian monsoon in a changing climate. Adv Atmos Sci, 36: 887–901

Chowdary J S, Hu K, Srinivas G, Kosaka Y, Wang L, Rao K K. 2019. The Eurasian jet streams as conduits for East Asian monsoon variability. Curr Clim Change Rep, 5: 233–244

Ding R, Ha K J, Li J. 2010. Interdecadal shift in the relationship between the East Asian summer monsoon and the tropical Indian Ocean. Clim Dyn, 34: 1059–1071

Ding Y, Liang P, Liu Y, Zhang Y. 2020. Multiscale variability of Meiyu and its prediction: A new Review. J Geophys Res Atmos, 125: e31496

Feng J, Wang L, Chen W. 2014. How does the East Asian Summer Monsoon behave in the decaying phase of El Niño during different PDO phases? J Clim, 27: 2682–2698

Fu C, Teng X. 1988. Climate anomalies in China associated with El Niño/Southern Oscillation (in Chinese). Chin J Atmos Sci, 12: 133–141

Ge Q S, Guo X F, Zheng J Y, Hao Z X. 2008. Meiyu in the middle and lower reaches of the Yangtze River since 1736. Chin Sci Bull, 53: 107–114

Ha Y, Zhong Z, Chen H, Hu Y. 2016. Out-of-phase decadal changes in boreal summer rainfall between Yellow-Huaihe River Valley and southern China around 2002/2003. Clim Dyn, 47: 137–158

Huang B, Thorne P W, Banzon V F, Boyer T, Chepurin G, Lawrimore J H, Menne M J, Smith T M, Vose R S, Zhang H M. 2017. Extended reconstructed sea surface temperature, Version 5 (ERSSTv5): Upgrades, validations, and intercomparisons. J Clim, 30: 8179–8205

Huang R, Chen J, Wang L, Lin Z. 2012. Characteristics, processes, and causes of the spatio-temporal variabilities of the East Asian monsoon system. Adv Atmos Sci, 29: 910–942

Kanamitsu M, Ebisuzaki W, Woollen J, Yang S K, Hnilo J J, Fiorino M, Potter G L. 2002. NCEP–DOE AMIP-II reanalysis (R-2). Bull Amer Meteor Soc, 83: 1631–1644

Lau K M, Lee J Y, Kim K M, Kang I S. 2004. The North Pacific as a regulator of summertime climate over Eurasia and North America. J Clim, 17: 819–833

Li J, Zheng F, Sun C, Feng J, Wang J. 2019. Pathways of influence of the northern hemisphere mid-high latitudes on East Asian climate: A review. Adv Atmos Sci, 36: 902–921

Li T, Wang B, Wu B, Zhou T, Chang C P, Zhang R. 2017. Theories on formation of an anomalous anticyclone in western North Pacific during El Niño: A Review. J Meteorol Res, 31: 987–1006

Liang P, Chen L, Ding Y, He J, Zhou B. 2018. Relationship between long-term variability of Meiyu 560 over the Yangtze River and ocean and Meiyu's predictability study (in Chinses). Acta Meteorol Sin, 76: 379–393

Liang P, Ding Y. 2012. Climatologic characteristics of the intraseasonal oscillation of East Asian meiyu (in Chinses). Acta Meteorol Sin, 70: 418–435

Liu B, Yan Y, Zhu C, Ma S, Li J. 2020. Record-breaking Meiyu rainfall around Yangtze River in 2020 regulated by the subseasonal phase transition of North Atlantic Oscillation. Geophys Res Lett, 47: e90342

Liu Y, Chiang J C H. 2012. Coordinated abrupt weakening of the Eurasian and North African monsoons in the 1960s and links to extratropical North Atlantic cooling. J Clim, 25: 3532–3548

Mantua N J, Hare S R. 2002. The Pacific decadal oscillation. J Oceanogr, 58: 35–44

Mantua N J, Hare S R, Zhang Y, Wallace J M, Francis R C. 1997. A Pacific interdecadal climate oscillation with impacts on salmon production. Bull Amer Meteor Soc, 78: 1069–1079

Neale R B, Gettelman A, Lauritzen P H, Park S, Williamson D, Conley A, Garcia R, Kinnison D, Lamarque J F, Marsh D, Mills M, Smith A, Tilmes S, Vitt F, Morrison H, Cameron-Smith P, Collins W, Iacono M J, Easter R, Ghan S, Liu X, Rasch P, Taylor M. 2012. Description of the NCAR Community Atmosphere Model (CAM 5.0). NCAR Tech Note NCAR/TN-486+STR, 289

Pan Y, Shen Y, Yu J, Xiong A. 2015. An experiment of high-resolution gauge-radar-satellite combined precipitation retrieval based on the Bayesian merging method (in Chinses). Acta Meteorol Sin, 73:177–186

Saji N H, Goswami B N, Vinayachandran P N, Yamagata T. 1999. A dipole mode in the tropical Indian Ocean. Nature, 401: 360–363

Schlesinger M E, Ramankutty N. 1994. An oscillation in the global climate system of period 65–70 years. Nature, 367: 723–726

Si D, Ding Y. 2016. Oceanic forcings of the interdecadal variability in east Asian summer rainfall. J Clim, 29: 7633–7649

Si D, Ding Y H, Liu Y J. 2009. Decadal northward shift of the Meiyu belt and the possible cause. Sci Bull, 54: 4742–4748

Sun B, Wang H, Zhou B, Li H. 2019. Interdecadal variation in the synoptic features of Mei-Yu in the Yangtze river valley region and relationship with the pacific decadal oscillation. J Clim, 32: 6251–6270

Wang B, Lin H. 2002. Rainy season of the Asian–Pacific summer monsoon. J Clim, 15: 386–398

Wang B, Wu R, Fu X. 2000. Pacific-East Asian teleconnection: How does ENSO affect East Asian climate? J Clim, 13: 1517–1536

Wang B, Wu R, Lau K M. 2001. Interannual variability of the asian summer monsoon: Contrasts between the Indian and the Western North Pacific-East Asian monsoons. J Clim, 14: 4073–4090

Watanabe M, Jin F. 2002. Role of Indian Ocean warming in the development of Philippine Sea anticyclone during ENSO. Geophys Res Lett, 29: 116-1–116-4

Wei F, Xie X. 2005. Interannual and interdecadal oscillations of Meiyu over the middle lower reaches of the Chang-Jiang River for 1885–2000 (in Chinese). J Applied Meteorol Sci, 16: 492–499

Wu B, Li T, Zhou T. 2010. Relative contributions of the Indian Ocean and local SST anomalies to the maintenance of the western North pacific anomalous anticyclone during the El Niño decaying summer. J Clim, 23: 2974–2986

Wu B, Zhou T, Li T. 2009. Seasonally evolving dominant interannual variability modes of East Asian climate. J Clim, 22: 2992–3005

Xie M, Wang C. 2020. Decadal variability of the anticyclone in the Western North Pacific. J Clim, 33: 9031–9043

Xie P, Yatagai A, Chen M, Hayasaka T, Fukushima Y, Liu C, Yang S. 2007. A gauge-based analysis of daily precipitation over East Asia. J Hydrometeorol, 8: 607–626

Xie S P, Hu K, Hafner J, Tokinaga H, Du Y, Huang G, Sampe T. 2009.

Indian Ocean capacitor effect on Indo–Western Pacific climate during the summer following El Niño. J Clim, 22: 730–747
Xie X, Wang H, Liu X, Li J, Wang Z, Liu Y. 2016. Distinct effects of anthropogenic aerosols on the East Asian summer monsoon between multidecadal strong and weak monsoon stages. J Geophys Res Atmos, 121: 7026–7040
Xu P, Wang L, Chen W, Feng J, Liu Y. 2019. Structural changes in the Pacific–Japan pattern in the late 1990s. J Clim, 32: 607–621
Yang J, Qian Y. 2009. Temporal evolution of 121a Meiyu series. Sci Meteorol Sin, 29: 285–290
Zhang Y, Wallace J M, Battisti D S. 1997. ENSO-like interdecadal variability: 1900–93. J Clim, 10: 1004–1020
Zhang H, Wen Z, Wu R, Chen Z, Guo Y. 2017. Inter-decadal changes in the East Asian summer monsoon and associations with sea surface temperature anomaly in the South Indian Ocean. Clim Dyn, 48: 1125–1139
Zhang R, Sumi A, Kimoto M. 1996. Impact of El Nino on the East Asian Monsoon: A diagnostic study of the ’86/87 and ’91/92 events. J Meteorol Soc Jpn, 74: 49–62
Zhu Y, Wang H, Ma J, Wang T, Sun J. 2015. Contribution of the phase transition of Pacific Decadal Oscillation to the late 1990s’ shift in East China summer rainfall. J Geophys Res Atmos, 120: 8817–8827
Zhu Z, Li T, He J. 2014. Out-of-Phase relationship between boreal spring and summer decadal rainfall changes in southern China. J Clim, 27: 1083–1099

(Responsible editor: Xiuqun YANG)